



ELSEVIER

Contents lists available at ScienceDirect

Journal of Hydrology

journal homepage: www.elsevier.com/locate/jhydrol

Research papers

Importance of variability in initial soil moisture and rainfalls on slope stability



Jing-Sen Cai^a, Tian-Chyi Jim Yeh^{b,c,*}, E-Chuan Yan^a, Rui-Xuan Tang^a, Yong-Hong Hao^b, Shao-Yang Huang^d, Jet-Chau Wen^e

^a Faculty of Engineering, China University of Geosciences, Wuhan 430074, China

^b Tianjin Key Laboratory of Water Resources and Environment, Tianjin Normal University, Tianjin, China

^c Department of Hydrology and Atmospheric Sciences, University of Arizona, Tucson, AZ 85721, USA

^d Graduate School of Engineering Science and Technology, National Yunlin University of Science and Technology, Douliou, Taiwan

^e Research Center for Soil and Water Resources and Natural Disaster Prevention, National Yunlin University of Science and Technology, Douliou, Taiwan

ARTICLE INFO

This manuscript was handled by Corrado Corradini, Editor-in-Chief, with the assistance of Rao S. Govindaraju, Associate Editor

Keywords:

Slope stability uncertainty

Variability

Initial soil pore water pressure

Rainfall characteristics

Large-uncertainty zone

Low-reliability zone

ABSTRACT

A first-order moment analysis is developed to investigate the temporal and spatial propagation of uncertainty of slope stability during rainfall, considering spatial variabilities in initial soil water pressure and soil hydraulic properties, and temporal variability of rainfall. Results of the analysis indicate that the uncertainties resulting from variabilities in initial soil pore water pressure distributions and rainfalls are comparable with that from the variability in soil hydraulic properties. Further, the evolution of slope stability uncertainty is driven by the mean flow field, and a localized large-uncertainty zone along the slope profile could form, leading to a localized low-reliability zone, which may lead to the failure of the slope. In particular, when the slope is close to saturation, the reliability of the stability analysis of any elevation of the slope is low even at early rainfall times. On the other hand, when the slope is unsaturated and heavy rainfalls occur, the low-reliability zone exists at shallow parts of the slope at early times. The results also show that greater unreliability exists at shallow depths at early times when the rainfall has a descending trend in comparison with uniform and increasing trend. Lastly, the low-reliability zone is always near the impermeable bedrock if rainfall persists.

1. Introduction

Rainfall-induced landslides are one of the most severe natural disasters (Ng and Shi, 1998; Ng et al., 2001). Significant landslide disasters triggered by rainfalls have been reported annually in many parts of the world such as Brazil, Italy, South Africa, Japan and China (Chowdhury and Flentje, 2002). Infiltration of precipitation increases soil moisture content, decreases matric suction of unsaturated soils or creates positive pore water pressure, and in turn, decreases the shear strength of soils, and consequently, leads to landslides. Preventions for geohazards such as slope failures and landslides, therefore, require reliable evaluations of slope stability under rainfall infiltrations.

Rainfall-induced landslides are attributed to geologic characteristics, topography, initial soil pore water pressure, and precipitation of the slope area. Due to the heterogeneous nature of the geology and our inability to characterize them, an increasing number of researches has

focused on the variabilities of soil properties and their effects on the slope stability (e.g., Ali et al., 2014; Cai et al., 2017a,c,d; Cho, 2014; Griffiths et al., 2011; Gui et al., 2000). On the other hand, precipitation and initial soil pore water pressure generally exhibit a high degree of temporal and spatial variabilities. For instance, it has been widely recognized that rainfall intensity is significantly higher on the escarpment relative to the coastal plain (Chowdhury and Flentje, 2002). In addition, rainfall processes are known to vary widely in time. That is, spatiotemporal variability is an intrinsic characteristic of climate (Paolini et al., 2005). Furthermore, the distribution of initial soil pore water pressures in the slope also varies spatially due to variabilities in prior rainfalls and heterogeneities of geology.

Previous studies have focused on the variabilities in rainfalls or initial soil pore water pressure distributions. For example, D'Odorico (2005) showed that the temporal variations of rainfall intensity affect stability, and the rainfall pattern with a peak at the end of the rainfall

* Corresponding author at: Tianjin Key Laboratory of Water Resources and Environment, Tianjin Normal University, 393 Binshuixidao Road, Xiqing District, Tianjin 300387, China.

E-mail address: cjs619242601@gmail.com (J.-S. Cai), yeh@hwr.arizona.edu (T.-C. Jim Yeh).

¹ Department of Hydrology and Atmospheric Sciences, The University of Arizona, 1133 E. James E. Rogers Way, 122 Harshbarger Bldg 11, Tucson, AZ 85721, USA.

<https://doi.org/10.1016/j.jhydrol.2019.01.046>

Received 14 November 2018; Received in revised form 1 January 2019; Accepted 14 January 2019

Available online 02 February 2019

0022-1694/ © 2019 Elsevier B.V. All rights reserved.

process has a stronger destabilizing effect than a constant rainfall. Minder et al. (2009) studied the impact of spatial rainfall heterogeneity on landslide susceptibility based on a numerical model and pointed out that the heterogeneous rainfall decreased slope stability. von Ruetze et al. (2014) investigated the effects of rainfall variabilities and initial soil hydraulic conditions on the statistics of locations, the numbers, and the released volumes of landslides at a catchment. They suggested that fewer landslides were triggered under dry initial soil conditions than the wet conditions, and rainfall heterogeneity may be an important missing link required for landslide prediction.

Since it is practically impossible to characterize the variabilities in initial soil pore water pressure and rainfalls in detail, uncertainties in the evaluation of slope stability exist. For this reason, these variabilities deserve particular attention. The understanding of these variabilities and their effects on slope stability is still relatively limited at present. For instance, in most studies, rainfall data is obtained via spatially and temporally averaging approaches or interpolation using sparse rain gauge measurements or coarse rainfall radar information over large areas (von Ruetze et al., 2014). The initial soil pore water pressure is frequently assumed to be spatially invariant (e.g., Cho, 2014) or to be those obtained by steady-state simulations under antecedent rainfalls (e.g., Cai et al., 2017b). In these approaches, the initial soil pore water pressure and rainfall are considered as deterministic, and their uncertainties are ignored. These simplifications lead to inaccurate predictions of landslides, which hamper mitigation procedures.

During this rainfall-infiltration process in a slope, the effect of spatial variability in initial soil pore water pressure and soil properties, and temporal varying rainfall on the slope stability evolves with time and space. As a result, it becomes important to know where and when the potential slip surfaces have relatively large uncertainties of their stabilities and whether these uncertainties are significant enough to impact the slope stability. These issues are seldom investigated. Therefore, we are compelled to conduct a probabilistic analysis of the interaction between temporal and spatial distributions of initial soil pore water pressures, rainfalls, soil properties, and slope stability.

The primary objective of this study is to propose a stochastic approach for a better understanding and prediction of the temporal and spatial evolution of slope stability uncertainty caused by variabilities in initial soil pore water pressure distributions, rainfalls, and soil hydraulic properties and its importance in slope stability evaluations during rainfall.

This paper is organized as follows. The basic equations for describing the one-dimensional vertical seepage and evaluation of infinite slope stability and deterministic analysis of slope stability are presented in Section 2. Section 3 first presents the first-order moment approach and the approach to quantitatively represent the spatial variability in initial hydraulic conditions and soil hydraulic properties and the temporal variability of rainfalls during the rainfall process. Then, it describes a probabilistic analysis of slope stability. Simulation results for different scenarios are discussed in Section 4 with respect to the effects of the initial soil pore water pressure, rainfall intensity, rainfall duration and rainfall pattern on uncertainty propagations of slope stability and the importance of these uncertainties on slope stability. The article then draws conclusions in Section 5.

2. Deterministic slope stability analysis under rainfall

2.1. Governing equations for seepage analysis

The rainfall infiltration process in the infinite slope (Fig. 1) is assumed to be described by a one-dimensional governing vertical flow equation (Yeh et al., 2015):

$$\frac{\partial}{\partial z} \left(K(h) \left(\frac{\partial h}{\partial z} + 1 \right) \right) = [\eta S_s + C(h)] \frac{\partial h}{\partial t} \quad (1)$$

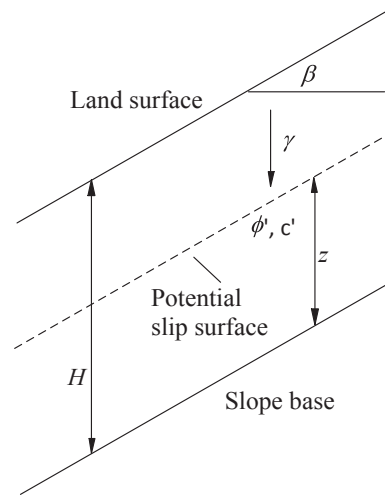


Fig. 1. An infinite slope model.

where z denotes the coordinate along the vertical z -axis (positive upward); h is the pressure head; $K(h)$ is the hydraulic conductivity; S_s is the specific storage; $C(h)$ denotes the moisture capacity term; t denotes time; η is the saturation index. h is a positive value if the medium is fully saturated and is negative if the medium is unsaturated. $K(h)$ varies with pressure head under unsaturated conditions. S_s represents the percentage of water released from a unit volume of fully saturated porous media under a unit decline in hydraulic head. On the other hand, $C(h) = \frac{\partial \theta}{\partial h} \Big|_h$ is the change in moisture content in a unit volume of the porous medium under a unit change of negative pressure head, when the medium is unsaturated. While S_s and $C(h)$ are similar in definition, the physical mechanisms they represented are entirely different. S_s is related to the compressibility of porous media and water while the medium remains fully saturated, whereas $C(h)$ represents desaturation or saturation of the pores in the medium. On the right-hand side of Eq. (1), η is set to 1 if the medium is saturated and 0 if the medium is unsaturated.

Eq. (1) is subjected to an initial condition:

$$h(z, 0) = h_0(z) \quad (2a)$$

where $h_0(z)$ is the prescribed pressure head at the location z at the initial time.

The boundary conditions for Eq. (1) are: at the land surface, a prescribed pressure head h_b at the time t is assigned to the top boundary to represent rainfall for the infinite slope:

$$h(H, t) = h_b(t) \quad (2b)$$

while at slope base, no flux boundary is utilized:

$$K(h) \left(\frac{\partial h}{\partial z} + 1 \right) \Big|_{(0,t)} = 0 \quad (2c)$$

To simulate flow in a hillslope using the governing equation and its initial and boundary conditions, the hydraulic conductivity-pressure constitutive relationship by Mualem(1976) and the moisture-pressure head constitutive relationship by van Genuchten(1980), known as the MVG model, are adopted. They are listed below:

$$K(h) = \begin{cases} K_s (1 - (\alpha_1 |h|)^{\alpha_2 - 1} [1 + (\alpha_1 |h|)^{\alpha_2}]^{-\alpha_3})^2 & h < 0 \\ [1 + (\alpha_1 |h|)^{\alpha_2}]^{(-\alpha_3/2)} K_s & h \geq 0 \end{cases} \quad (3)$$

$$\theta(h) = \begin{cases} (\theta_s - \theta_r) [1 + (\alpha_1 |h|)^{\alpha_2}]^{-\alpha_3} + \theta_r & h < 0 \\ \theta_s & h \geq 0 \end{cases} \quad (4)$$

where α_1 , α_2 and α_3 are soil parameters and $\alpha_3 = 1 - 1/\alpha_2$; K_s is the

saturated hydraulic conductivity; θ_s and θ_r denote the saturated and residual volumetric moisture contents, respectively.

2.2. Governing equations for slope stability analysis

The factor of safety along i th potential slip surface (i.e., FS_i) of an infinite slope has been widely evaluated using the limit equilibrium model (LEM) with the unified effective stress under both saturated and unsaturated conditions (Lu and Godt, 2008). If we let the pore air pressure u_a be atmospheric pressure (i.e., $u_a = 0$), FS_i can be expressed as (e.g., Ali et al., 2014; Cho, 2014; Griffiths et al., 2011; Li et al., 2014):

$$FS_i = \frac{((H - z_i)\gamma_i \cos^2 \beta - \sigma_i^s) \tan \phi'_i + c'_i}{(H - z_i)\gamma_i \sin \beta \cos \beta} + \frac{c'_i}{(H - z_i)\gamma_i \sin \beta \cos \beta} \quad (0 \leq z_i < H; i = 1, \dots, n) \quad (5)$$

where n is the total number of potential slip surfaces; β is the slope inclination; γ_i is the averaged total unit weight above i th potential slip surface; H denotes the vertical distance of soils from the slope base to the land surface; c'_i and ϕ'_i are the effective cohesion and the effective soil friction angle at i th potential slip surface, and z_i is the elevation (positive upward) of i th potential slip surface (see Fig. 1); σ_i^s represents the effective negative pore water pressure under unsaturated conditions or effective positive pore water pressure when under saturated conditions at i th potential slip surface (Lu and Godt, 2008).

According to Lu and Godt (2008), σ_i^s can be expressed as:

$$\sigma_i^s = -\frac{\theta_i - \theta_r}{\theta_s - \theta_r}(u_a - u_{wi}) = -S_{ei}(u_a - u_{wi}) \quad (6)$$

where u_{wi} , S_{ei} and θ_i are the pore water pressure, the effective water saturation and the volumetric moisture content at i th potential slip surface, respectively. The relationship between u_w and h is $u_w = h\gamma_w$. $\sigma_i^s = S_{ei}u_{wi} < 0$ is for unsaturated conditions ($u_{wi} < 0$), and $\sigma_i^s = u_{wi} \geq 0$ is for saturated conditions ($u_{wi} \geq 0$). Via this unified effective stress theory, Eq. (5) can account for both the reduction in matric suction and the development of positive pore water pressure in a continuous form (Cho, 2014; Lu and Godt, 2008).

In this study, the variation in unit weight resulting from changes in moisture content during infiltration is evaluated by integration of the moisture content profile above the potential slip surface. That is, the total unit weight γ_i can be expressed as follows:

$$\gamma_i = \frac{1}{H - z_i} \int_{z_i}^H (\gamma_d + \theta(z)\gamma_w) dz \quad (0 \leq z_i < H) \quad (7)$$

where γ_d is the dry unit weight of the soil; γ_w is the unit weight of water.

2.3. Setup of model

Catastrophic shallow landslides frequently occur under heavy rainfall in weathered granite residual soil slopes in Korea and the southeast coast of China. The method developed here, therefore, is applied to the weathered granite residual soil slopes as an example. Generally, the hillslope in these areas can be treated as an unsaturated shallow layered slope above an impermeable bedrock, and the one-dimensional infinite slope model is appropriate for the simulation (e.g., Ali et al., 2014; Cai et al., 2017a,c,d; Cho, 2014; Griffiths et al., 2011; Li et al., 2014; Zhang et al., 2014). The geometrical parameters and all the hydraulic and mechanical parameters for this investigation are listed in Table 1. They are adopted from the data listed in Cho (2014), which are representative of typical weathered granite soils in Seochang, Korea.

The entire infinite slope is discretized into 40 elements in the vertical direction, representing 40 potential slip surfaces (i.e., $n = 40$) with an interval (Δz) of 0.05 m. These potential slip surfaces are numbered 1 to 40 from the slope base to the land surface (see Fig. 1). In addition,

Table 1

Statistics of h_0 , h_b and K_s , related parameters and slope geometrical parameters.

Parameters	Values
Mean of h_0 , μ_{h_0}	-2 m
Mean of h_b , μ_{h_b}	-0.1 m
Mean of K_s , μ_{K_s}	0.2592 m/d
COVs of h_0 , h_b and K_s	1
Correlation scale of h_0 in space, λ_{h_0}	0.3 m
Correlation scale of h_b in time, λ_{h_b}	0.3 day
Correlation scale of K_s in space, λ_{K_s}	0.3 m
Effective cohesion c' , $\mu_{c'}$	5.0 kN/m ²
Effective friction angle ϕ' , $\mu_{\phi'}$	32°
Specific storage, S_s	0.001 m ⁻¹
Saturated volumetric moisture content, θ_s	0.358
Residual volumetric moisture content, θ_r	3.58×10^{-4}
Coefficient 1 in VG model, α_1	0.5 m^{-1}
Coefficient 2 in VG model, α_2	1.289
Slope height, H	2 m
Slope angle, β	40°
Dry unit weight, γ_d	16 kN/m ³
Unit weight of water, γ_w	9.8 kN/m ³

the initial pressure head distribution in the slope is described by h_0 , which is a function of z , and an impermeable boundary is located at the slope base. As rainfall occurs, a specific pressure head, h_b , which is a function of t , is assigned to the top boundary to represent a variable rainfall.

A finite element analysis code (available at <http://tian.hwr.arizona.edu/downloads>, Yeh et al., 1993) is employed to simulate the one-dimensional vertical seepage described by Eq. (1), subjected to the initial and boundary conditions described by Eq. (2). Subsequently, computed vertical profiles of pore water pressure, effective water saturation and moisture content from transient finite element seepage analyses are used as inputs for calculating FS_i ($i = 1, \dots, n$) at each time step by Eq. (5).

2.4. Deterministic analysis

First, a deterministic transient seepage analysis is conducted, by using the mean values of parameters (i.e., μ_{h_0} , μ_{h_b} and μ_{K_s}) listed in Table 1, to study rainfall infiltration into the infinite slope with the impermeable boundary located at the slope base. The vertical profiles of pore water pressure, h , and the corresponding factor of safety FS_i at some selected times due to a given h_b (-0.1 m) are displayed in Fig. 2a and b, respectively. As shown in Fig. 2a, the wetting front propagates as rainfall infiltration continues until it reaches the slope base. The matric suction of the soil behind the wetting front gradually reduces over time, and the soil becomes fully saturated and soil water pressure becomes positive and increases afterward. The effect of infiltration on slope stability is illustrated in Fig. 2b, which shows that the advance of the wetting front decreases the factor of safety at each potential slip surface. At 1 day, the factor of safety of this slope decreases below 1 (i.e., unstable slope).

The above analysis based on the mean values of parameters provides a reference to illustrate the effects of variability of h_0 , h_b and K_s in a heterogeneous slope. First, realizations of random fields of h_0 , h_b and K_s (Fig. 2c and d) are generated using the Karhunen-Loève (K-L) expansion method (e.g., Ghanem and Spanos, 1991; Jiang et al., 2015; Lu and Zhang, 2007) with the given spatial statistics listed in Table 1. h_0 and h_b are assumed to be normally distributed while K_s is assumed to be log-normally distributed (e.g., Brejda et al., 2000; Fenton and Griffiths, 2008; Griffiths et al., 2011; Jiang et al., 2015; Li et al., 2014; Parkin et al., 1988; Parkin and Robinson, 1992; Phoon and Kulhaway, 1999). Note that various types of models, e.g., the multiplicative random cascade models (Gupta and Waymire, 1993; Menabde and Sivapalan,

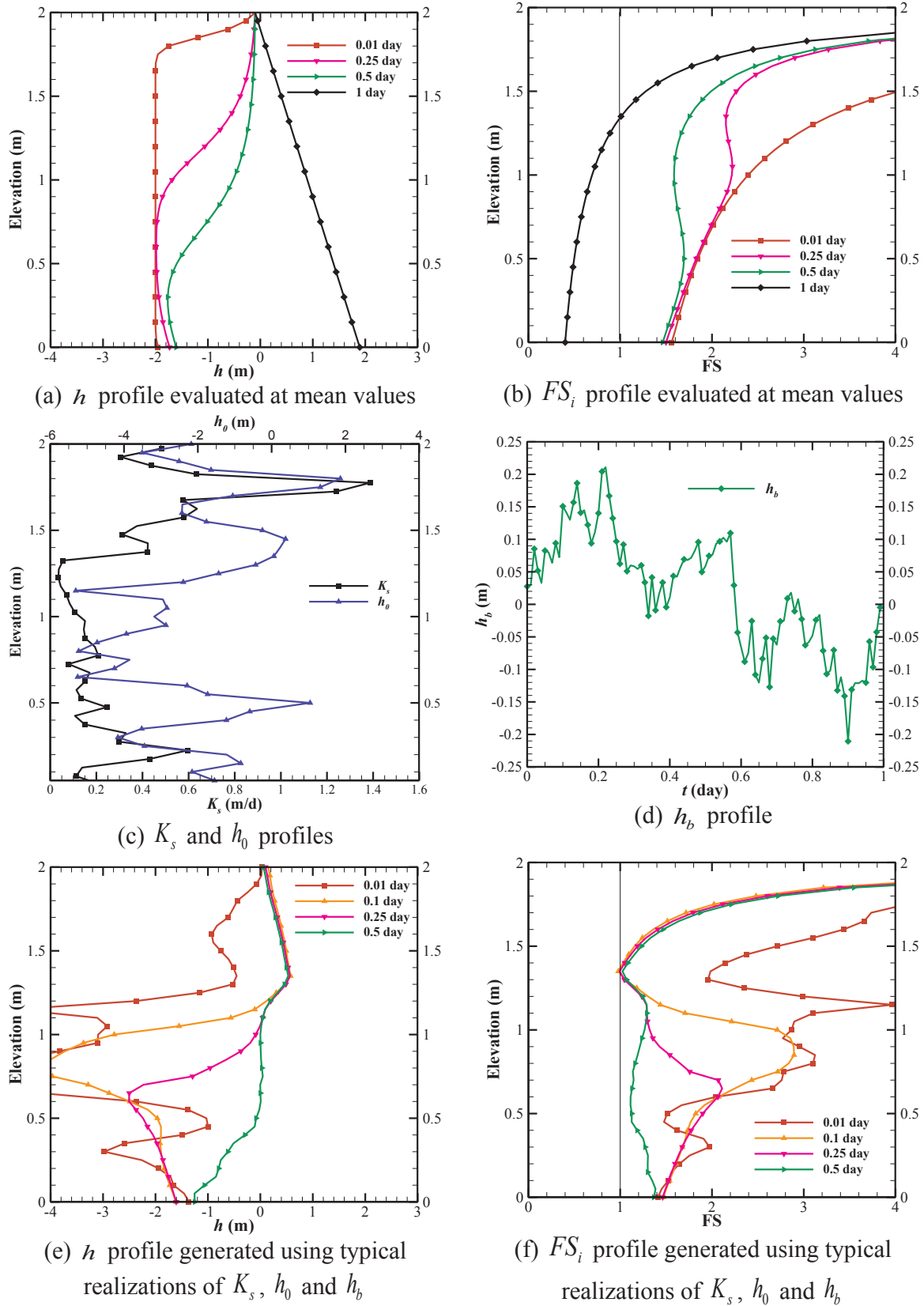


Fig. 2. Results of deterministic analyses.

2000), have been proposed in the literature for modeling rainfall time series. However, in this study, we treat h_b time series as a stochastic temporal process to illustrate the effect of variability in h_b . The

generated realization (see Fig. 2d) is sufficient to capture observed features of measured rainfall data reported in Stern and Coe (1984) and Menabde and Sivapalan (2000) such as intermittency and correlation.

In addition, considering the fact that the distributions of h_0 , K_s and h_b are generally unknown, in the study, h_0 is randomly generated and assumed to be uncorrelated with K_s and h_b at previous time periods (i.e., rainfall history). If these factors are known, correlation between these parameters could reduce the uncertainty of h_0 . For this reason, this assumption is deemed realistic.

Subsequently, the flow fields are simulated, stability analyses are conducted, and the results are displayed in Fig. 2e and f. According to the figures, the simulated h and FS_i profiles dramatically differ from those based on mean values of parameters (Fig. 2a and b), which represent the most likely h and FS_i profiles at different times. For example, the shape of h and FS_i profiles in Fig. 2e and f are erratic at 0.01 day due to the variability of h_0 . As the infiltration continues, their deviations from the most likely profiles at the corresponding times become larger. Such large differences thus may pose a threat to the stability of the slope (e.g., in Fig. 2f, the FS_i 's around Elevation 1.3 m are smaller than 1). For this reason, a slope stability analysis should consider uncertainties in the variability of antecedent moisture content, in the temporal variability of rainfalls and in the spatial variability of soil properties (e.g., K_s).

3. Probabilistic slope stability analysis

In order to address the uncertainty issue as presented above, a first-order moment approach (Cai et al., 2017d, 2016) is developed and described below.

3.1. First-order estimation of slope stability uncertainty

The initial pressure head, h_0 , which is directly related to soil moisture content, varies spatially and its distribution is unknown. We can treat it as a spatial random field. This means the initial pressure head $h_0(z_i)$ at each location in the slope is a random variable, which has a mean value and a variance. The collection of these random variables (i.e., $h_0(z_i), i = 1, \dots, n$) forms the random field and is characterized by a joint probability distribution (see Yeh et al., 2015). Therefore, $h_0(z_i)$ is expressed in terms of the mean and perturbations:

$$h_0(z_i) = \mu_{h_0} + p_{h_0}(z_i) \quad (i = 1, \dots, n) \tag{8a}$$

where μ_{h_0} is the mean of h_0 and $p_{h_0}(z_i)$ denotes the perturbation of h_0 at the location z_i .

The pressure head h_b at the land surface, which is related to rainfall, changes with time t and its distribution is also unknown. Thus, h_b at each time t_l is considered as a random variable, denoted as $h_b(t_l)$, which has a mean value and a variance, representing the uncertainty due to the temporal variability as well as lack of measurements. Consequently, h_b can be expressed as:

$$h_b(t_l) = \mu_{h_b}(t_l) + p_{h_b}(t_l) \quad (l = 1, \dots, m) \tag{8b}$$

where $\mu_{h_b}(t_l)$ is the time-varying mean of h_b , $p_{h_b}(t_l)$ denotes the perturbation of h_b at the time t_l and m denotes the total number of discrete time.

In addition, the medium property K_s of the slope is also considered as a spatial random field, which can be expressed in the form of the mean and perturbations:

$$K_s(z_i) = \mu_{K_s} + p_{K_s}(z_i) \quad (i = 1, \dots, n) \tag{8c}$$

where μ_{K_s} is the mean of K_s and $p_{K_s}(z_i)$ denotes the perturbation of K_s at location, z_i .

Likewise, the uncertainty in the FS_i is represented by $FS_i = \mu_{FS_i} + p_{FS_i}$, where μ_{FS_i} is the mean and p_{FS_i} is the perturbation. Expanding the FS_i in Eq. (5) in a Taylor series about the mean values of parameters, neglecting second-order and higher order terms, and subtracting the mean part from both sides, the FS_i at i th potential slip surface at a given time t can be approximately expressed in a matrix form as:

$$\mathbf{p}_{FS}(t) = \mathbf{J}_{FS h_0}(t)\mathbf{p}_{h_0} + \mathbf{J}_{FS h_b}(t)\mathbf{p}_{h_b} + \mathbf{J}_{FS K_s}(t)\mathbf{p}_{K_s} \tag{9}$$

where \mathbf{p}_{FS} , \mathbf{p}_{h_0} and \mathbf{p}_{K_s} are $n \times 1$ vectors; \mathbf{p}_{h_b} is a $m \times 1$ vector. $\mathbf{J}_{FS h_0}$ and $\mathbf{J}_{FS K_s}$ is a $n \times n$ Jacobian matrix, representing the change in $FS_i (i = 1, \dots, n)$ at i th potential slip surface at the time t due to a unit change in h_0 and K_s , respectively, at the location $z_j (j = 1, \dots, n)$ in the domain; $\mathbf{J}_{FS h_b}$ is a $n \times m$ Jacobian matrix, each term in the matrix denotes the sensitivity of $FS(z_i, t) (i = 1, \dots, n)$ to the change of h_b at the time $t_l (l = 1, \dots, m)$. Due to the nonlinearity, these sensitivities of the FS_i with respect to h_0, h_b or K_s need to be evaluated numerically. In this study, the perturbation approach is employed. We refer to Cai et al. (2017d) for derivations of this sensitivity analysis approach.

In this study, we assume that the spatially varying initial pressure head, h_0 , the time-varying boundary condition, h_b and the medium property K_s are mutually independent of each other. Therefore, multiplying Eq. (9) by itself on both sides and taking the expected value of the product lead to the corresponding FS_i auto-covariance matrix \mathbf{R}_{FSFS} :

$$\begin{aligned} \mathbf{R}_{FSFS}(t) = & \mathbf{J}_{FS h_0}(t)\mathbf{R}_{h_0 h_0}\mathbf{J}_{FS h_0}^T(t) + \mathbf{J}_{FS h_b}(t)\mathbf{R}_{h_b h_b}\mathbf{J}_{FS h_b}^T(t) \\ & + \mathbf{J}_{FS K_s}(t)\mathbf{R}_{K_s K_s}\mathbf{J}_{FS K_s}^T(t) \end{aligned} \tag{10}$$

where the superscript T denotes the transpose. $\mathbf{R}_{h_0 h_0}$ and $\mathbf{R}_{K_s K_s}$ are $n \times n$ auto-covariance matrices for h_0 and K_s , respectively; $\mathbf{R}_{h_b h_b}$ is an $m \times m$ auto-covariance matrix for h_b . $\mathbf{R}_{h_0 h_0}$ and $\mathbf{R}_{K_s K_s}$ are modeled using an exponential function (e.g., Cai et al., 2016) with the spatial correlation scale $\lambda_s = \lambda_{h_0} = \lambda_{K_s}$ in the z direction. Spatial correlation scale represents the distance within which the parameters (i.e., $h_0(z_i)$ or $K_s(z_i)$) are correlated in space. $\mathbf{R}_{h_b h_b}$ is modeled using the exponential function with a temporal correlation scale $\lambda_t = \lambda_{h_b}$. This temporal correlation scale represents the time interval within which the h_b at different times are correlated in time. The diagonal components of \mathbf{R}_{FSFS} are the FS_i variances ($i = 1, \dots, n$) at the time t , which are denoted as $\sigma_{FS}^2(z_i, t) (i = 1, \dots, n)$. The $\sigma_{FS}^2(z_i, t)$ represents the uncertainty in FS_i at i th potential slip surface at the time t , due to variabilities in h_0 at $z_j (j = 1, \dots, n)$, h_b at $t_l (l = 1, \dots, m)$ and K_s at $z_j (j = 1, \dots, n)$.

3.2. Reliability of slope stability evaluation

In the probabilistic slope stability analysis, we use the reliability index (e.g., Christian et al., 1994; Li et al., 2014) to represent the reliability of slope stability evaluation. The reliability index is defined as:

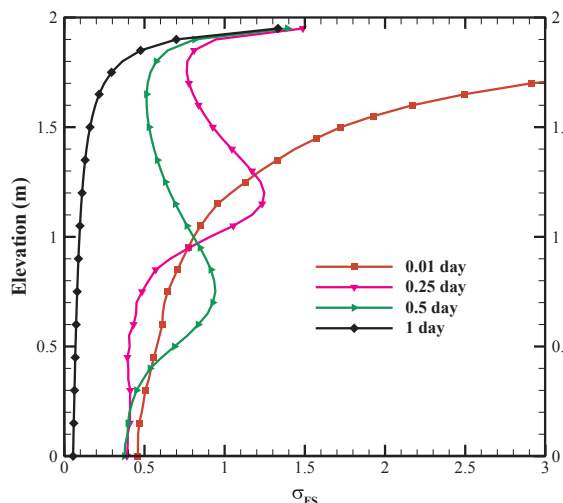
$$\beta_i(t) = (\mu_{FS_i}(t) - 1) / \sigma_{FS_i}(t) \tag{11}$$

where μ_{FS_i} and σ_{FS_i} are the mean and standard deviation of FS_i at the i th potential slip surface at the time t , respectively. The reliability index describes the reliability of stability evaluations at certain parts at the time t in the slope. It is defined as the ratio of the deviation of the mean FS from the limit equilibrium state value of 1.0 at a location i to the FS standard deviation at the location. According to Eq. (11), if the β_i at the i th surface is greater than 1, the standard deviation of the FS_i is small compared with the deviation between the mean FS_i and the critical equilibrium value 1. Therefore, the reliability of the slope is large. In other words, the uncertainty in slope stability due to variabilities in h_0, h_b and K_s is negligible and the μ_{FS_i} value, thus, is adequate to represent the slope stability. On the contrary, if the β_i is smaller than 1 at the time t , the distance between μ_{FS_i} and 1 is smaller than σ_{FS_i} . Hence, the uncertainty in slope stability at the time t is significant. This uncertainty is very likely to threaten the reliability of slope stability evaluations and deserves special attention.

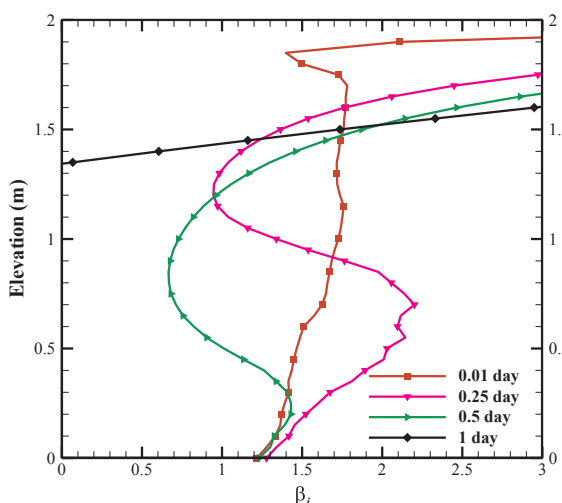
The $\mu_{FS_i} (i = 1, \dots, n)$ at each time step is evaluated using mean values of parameters and the $\sigma_{FS_i} (i = 1, \dots, n)$ at each time step is estimated using the first order moment approach abovementioned. Afterward, $\beta_i (i = 1, \dots, n)$ at each time step during rainfall is calculated by Eq. (11).

3.3. Probabilistic analysis for the base set

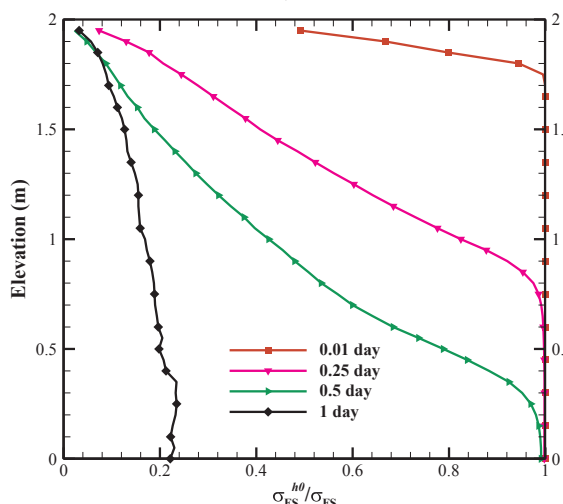
Here, a case with $\mu_{h_0} = -2$ m, $\mu_{h_b} = -0.1$ m, $\mu_{K_s} = 0.2592$ m/d,



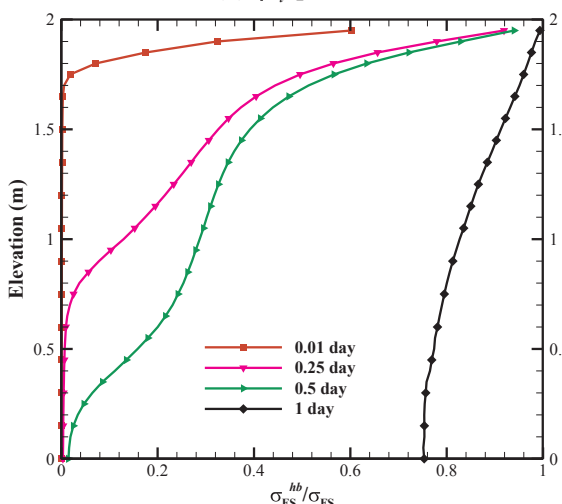
(a) σ_{FS_i} profiles



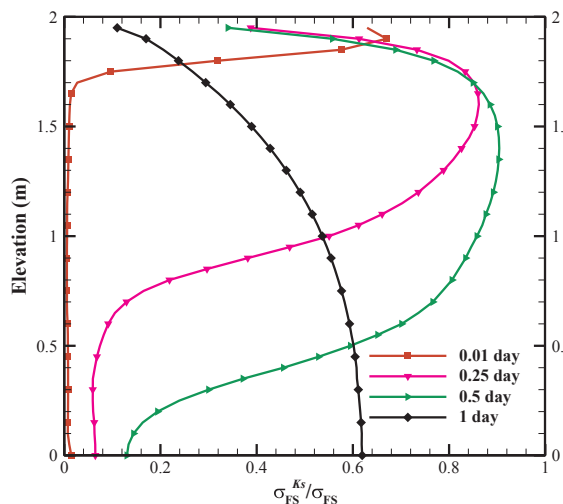
(b) β_i profiles



(c) Normalized σ_{FS_i} profiles due to variation of h_0



(d) Normalized σ_{FS_i} profiles due to variation of h_b



(e) Normalized σ_{FS_i} profiles due to variation of K_s

Fig. 3. σ_{FS_i} 's and β_i 's at different potential slip surfaces at the selected times for the base set.

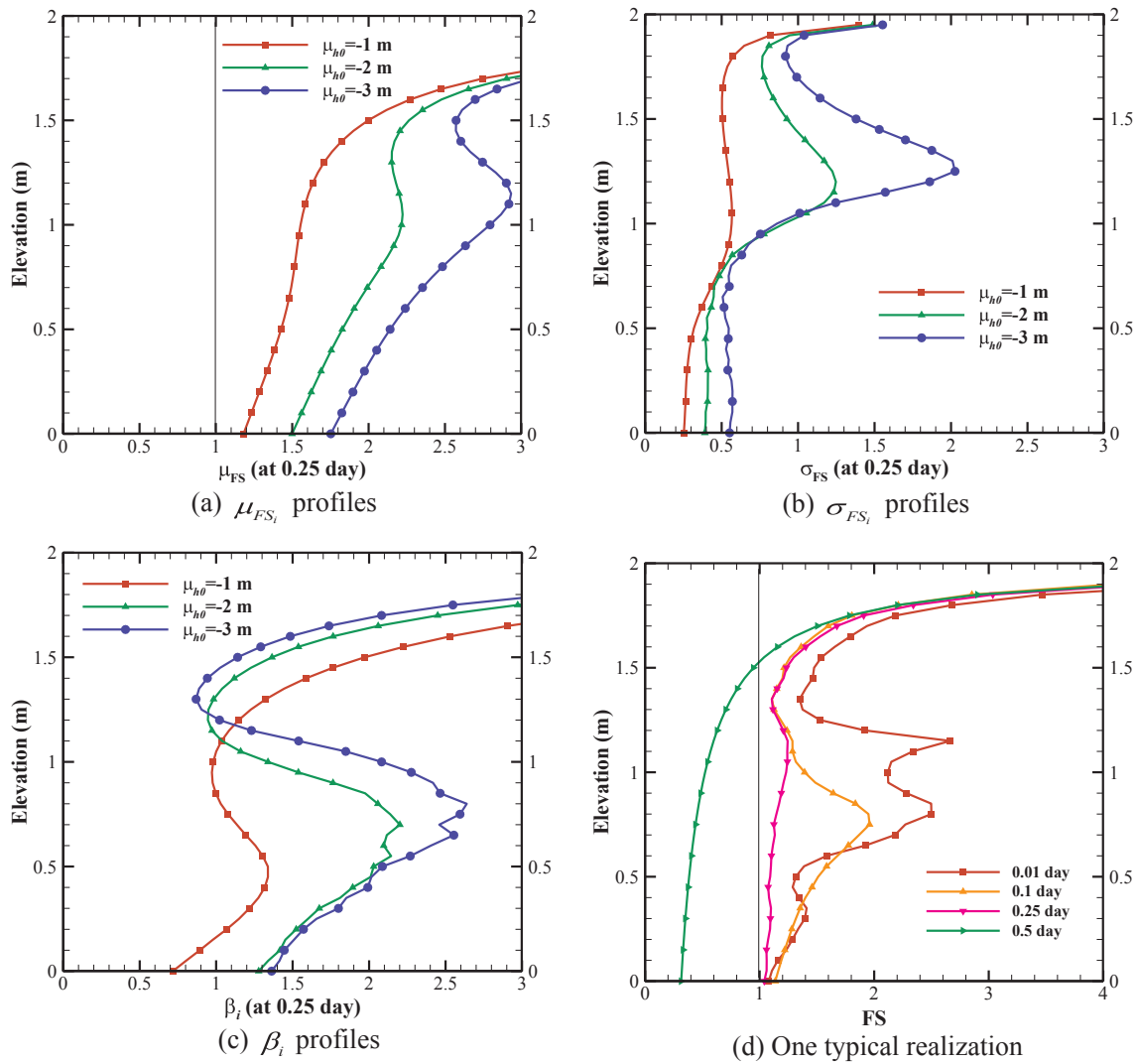


Fig. 4. μ_{FS_i} 's, σ_{FS_i} 's and β_i 's at different potential slip surfaces at the selected time ($t = 0.25$ day) with different mean initial pore water pressure distribution.

$COV_{h_0} = COV_{h_b} = COV_{K_s} = 1.0$, $\lambda_{h_0} = 0.3$ m, $\lambda_{h_b} = 0.3$ day and $\lambda_{K_s} = 0.3$ m is considered as the base case. Other parameters are listed in Table 1, and the rainfall duration is 1 day.

The spatial distributions of σ_{FS_i} and β_i at every potential slip surface of the slope under the variability of all parameters (h_0 , h_b and K_s) at four different times (0.01, 0.25, 0.5, 1 day) are depicted in Fig. 3a and b. The contribution to σ_{FS_i} from the variability of each parameter is presented in a normalized form in Fig. 3c–e. As illustrated in Fig. 3a, c–e, it is evident that the propagations of slope stability uncertainty due to impacts of variabilities in h_0 , h_b and K_s are driven by the mean flow field (see Fig. 2a and b). Since the mean value of rainfall intensity is larger than the value of initial pore water pressure and gravity, rainfall infiltrates into the slope and the uncertainties propagate downwards. At an early stage of infiltration (e.g., $t = 0.25$ day), the values of σ_{FS_i} 's at shallow depths are larger than those at deep parts. Further, the variations of h_0 and K_s contribute to σ_{FS_i} more than the variation of h_b does. Moreover, the variations of h_0 is the major uncertainty sources to σ_{FS_i} 's at deep parts of the slope. The variations of h_b and K_s only contribute to σ_{FS_i} at shallow depths.

At the late stage of infiltration (e.g., $t = 1$ day), the values of σ_{FS_i} at shallow depths decline and become smaller than those at deep parts. Meanwhile, the contribution of the variation of h_0 to σ_{FS_i} 's diminishes, while the contributions from the variations of h_b and K_s increase and become larger than that of h_0 . These results manifest the influence of

the variability in initial hydraulic condition at early times but its influence gradually attenuates as time progresses. On the other hand, the impact of the variability of rainfall continues to grow as the rainfall continues. Notice that although the contribution to σ_{FS_i} from variation of K_s is generally largest among these three uncertainty sources, the impacts on σ_{FS_i} from variations of h_0 and h_b are comparable with those from the variation of K_s and cannot be ignored. This finding illuminates the importance of characterization of the variability in initial hydraulic conditions and rainfalls in slope stability evaluation.

Notice that a localized large-uncertainty zone (i.e., the one along the solid purple line with gradient symbols at elevation 1.2 m in Fig. 3a) moves from shallow parts to deep parts of the slope and accumulates above the impermeable bedrock. This large-uncertainty zone greatly impacts the reliability of slope stability evaluations and deserves special attention. Fig. 3b indicates the rainfall infiltration decreases the β_i of each potential slip surface. For example, the minimum value of β_i 's is smaller than 1 at 0.25 day around elevation 1.2 m at shallow parts of the slope, and it decreases as infiltration continues. Overall, localized low-reliability zones form and move downwards during the rainfall infiltration process.

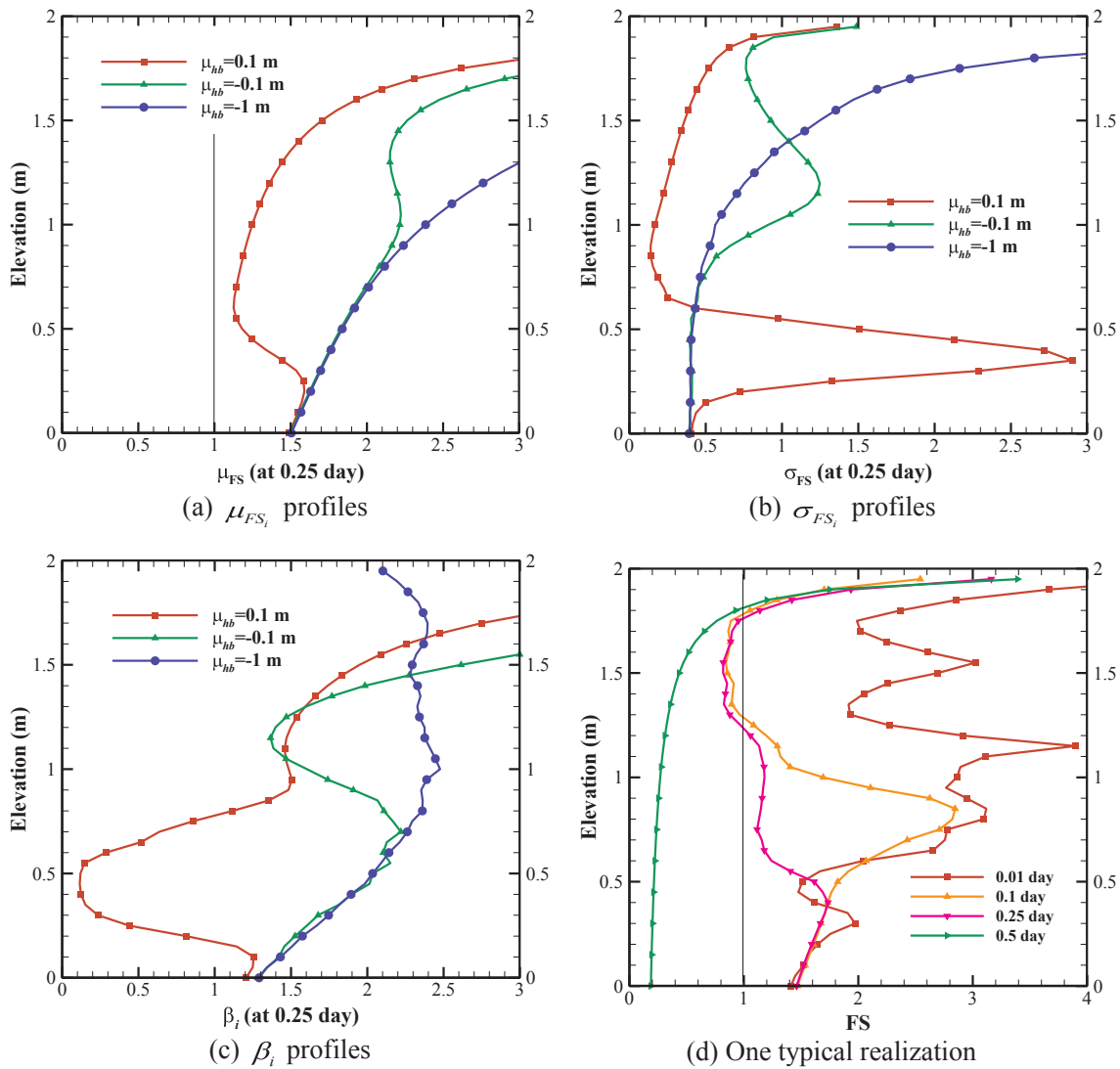


Fig. 5. μ_{FS_i} 's, σ_{FS_i} 's and β_i 's at different potential slip surfaces at the selected time ($t = 0.25$ day) under different rainfall intensities.

4. Influences of mean values of h_0 and h_b

4.1. Effects of initial pore water pressure

To investigate the effects of mean initial pore water pressure on slope reliability, three cases with μ_{h_0} equals -1 , -2 and -3 m, respectively, are considered. The COV_{h_0} 's of the three cases are set to the same, 1.0, and the COV_{h_b} , COV_{K_s} , λ_{h_0} , λ_{h_b} and λ_{K_s} of these cases are 1.0, 1.0, 0.3 m 0.3 day and 0.3 m, respectively. μ_{h_b} is set as -0.1 m, μ_{K_s} is 0.2592 m/d and the rainfall duration is 1 day.

As shown in Fig. 4a, where the μ_{FS_i} profiles at $t = 0.25$ day for the three cases are plotted, when the negative value of mean initial pore water pressure μ_{h_0} approaches zero, the mean values of FS_i 's of every potential slip surface decrease significantly and become closer to the limit equilibrium state (i.e., 1).

The σ_{FS_i} profiles at $t = 0.25$ day for the three cases due to variations of all parameters (h_0 , h_b and K_s) are displayed in Fig. 4b. The relative contribution from each parameter to σ_{FS_i} is shown in Fig. A1. Figs. 4b and A1 indicate that μ_{h_0} significantly influences the distributions of slope stability uncertainty induced by variabilities in initial hydraulic conditions, rainfalls, and soil hydraulic properties. That is, as μ_{h_0} increases (less negative), the localized large-uncertainty zone propagates rapidly to the deep parts of the slope under the same rainfall intensity owing to the high hydraulic conductivity resulting from high μ_{h_0} . In

addition, the maximum value of the uncertainty in the zone becomes smaller as μ_{h_0} increases. This result is consistent with the finding that the variance in pressure head generally decreases as soils become close to saturation, as explained by the moisture-dependent variability theory reported by Yeh et al. (1985a,b,c).

The reliability index β_i profiles at $t = 0.25$ day for the three cases are shown in Fig. 4c. Apparently, under the fixed rainfall intensity and time, the less saturation the slope is, the greater uncertainties of stabilities are near the shallow parts of slopes, and the minimum value of the localized reliability zone becomes smaller. All these factors lead to the high probability of failure at shallow parts of the less saturated slopes.

On the other hand, albeit the influence of variations in initial hydraulic conditions, rainfalls and soil hydraulic properties becomes smaller as the slope is close to saturation, the mean values of FS_i 's become small and the propagation of the impact of variations is speeded up. For these reasons, the likelihood of failure of the potential slip surfaces at any elevation increases. One typical realization of this situation is illustrated in Fig. 4d. This realization is generated with abovementioned statistics except μ_{h_0} is set as -1 m.

4.2. Effects of rainfall intensity

Here, the effects of the rainfall intensity on slope reliability are

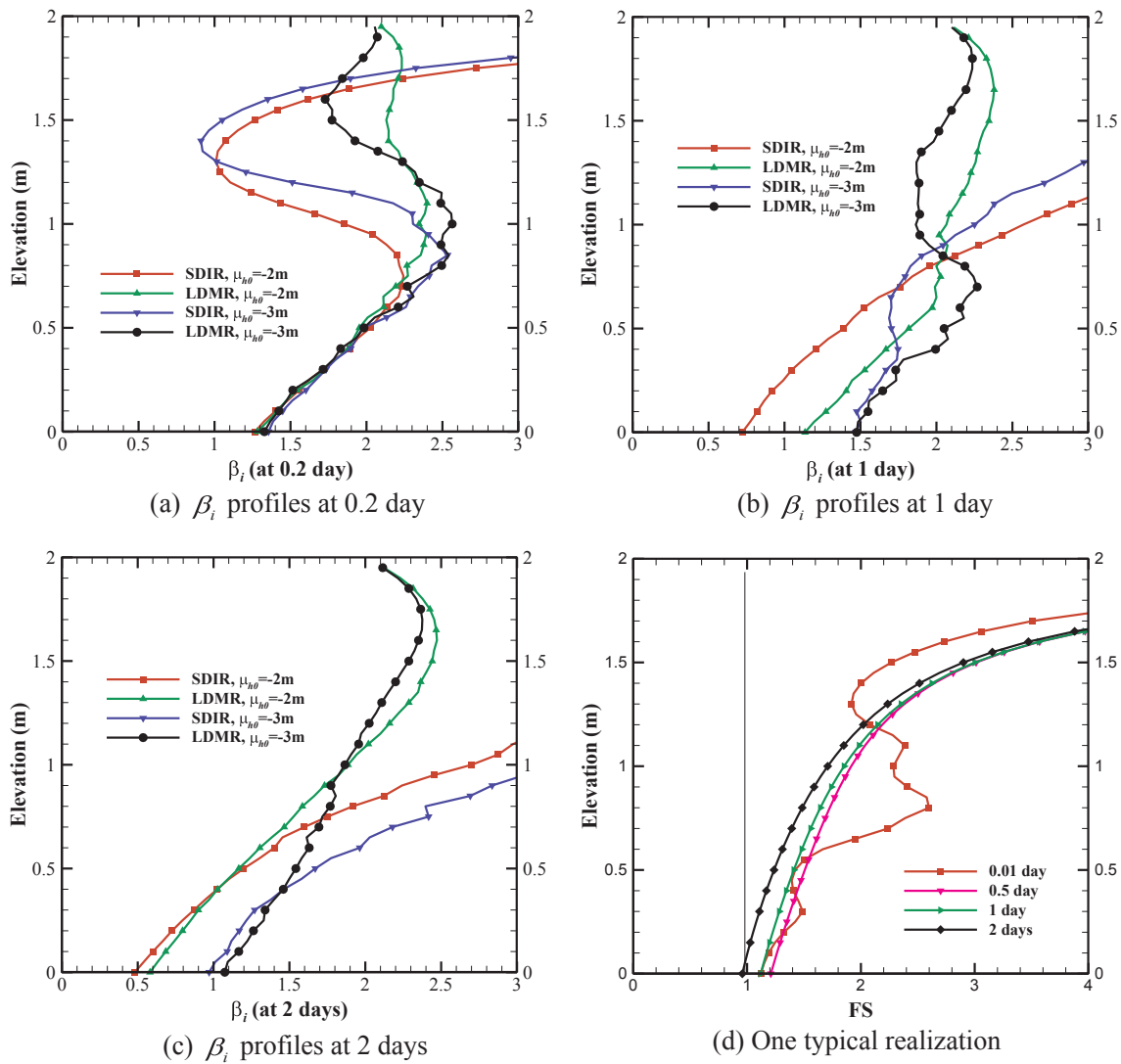


Fig. 6. β_i 's at different potential slip surfaces at different times with different rainfall durations.

studied through three cases with μ_{hb} equals 0.1, -0.1 and -1 m, respectively. COV_{h_0} , COV_{h_b} , COV_{K_s} , λ_{h_0} , λ_{h_b} and λ_{K_s} of these cases are 1.0, 1.0, 1.0, 0.3 m, 0.3 days and 0.3 m, respectively. The mean initial pore water pressure μ_{h_0} is set to be -2 m, μ_{K_s} is 0.2592 m/d and the rainfall duration is 1 day.

The μ_{FS_i} profiles at $t = 0.25$ day for the three cases are illustrated in Fig. 5a. As expected, the increase of the mean rainfall intensity μ_{hb} leads to decreases in μ_{FS_i} 's toward 1. Fig. 5b shows the σ_{FS_i} profiles at $t = 0.25$ day for the three cases due to variations of all parameters (h_0 , h_b and K_s) while the relative contribution from each parameter to σ_{FS_i} is shown in Fig. A2. As illustrated in these figures, μ_{hb} has significant impacts on the distributions of slope stability uncertainty. The increase in μ_{hb} leads to increasing trends in the propagation depth of σ_{FS_i} 's within the same time. In addition, given the same mean initial pore water pressure μ_{h_0} , larger μ_{hb} leads to a larger maximum value of the localized large-uncertainty zone. Moreover, when the mean rainfall intensity μ_{hb} becomes smaller and closer to μ_{h_0} , the localized large-uncertainty zone gradually vanishes. These findings indicate that a small rainfall intensity given limited times may fail to bring uncertainties into the slope. Under such circumstance, the σ_{FS_i} 's in the slope are mainly due to the variation of h_0 . Fig. 5c depicts the reliability index β_i profiles at $t = 0.25$ day for the three cases. As illustrated in Fig. 5c, given the same μ_{h_0} , the localized low-reliability zone gradually forms and the minimum value of the localized low-reliability zone becomes smaller as μ_{hb}

increases. This indicates that small rainfall intensities with short duration pose no threat to slope stability. On the other hand, under heavy rainfall conditions, the localized large-uncertainty zone first takes place at shallow parts of slopes: it impacts the reliability of slope stability evaluation and should be carefully treated. One typical realization of this situation is depicted in Fig. 5d. This realization is generated with abovementioned statistics except μ_{hb} is set as 0.1 m.

4.3. Effects of rainfall duration

In this section, we investigate the effects of rainfall duration on slope reliability. Four cases are examined, which include two types of rainfall (namely, short-duration, intense rainfall (SDIR) and long-duration, mild rainfall (LDMR)) on the slope under two initial hydraulic conditions. The SDIR is defined as the rainfall with a rainfall duration $t_{rainfall} = 0.2$ day and $\mu_{hb} = -0.1$ m, while the LDMR is rainfall with $t_{rainfall} = 2$ days and $\mu_{hb} = -1$ m. Two mean initial pore water pressure μ_{h_0} values (i.e., -2 m and -3 m, respectively) are considered. COV_{h_0} , COV_{h_b} , COV_{K_s} , λ_{h_0} , λ_{h_b} and λ_{K_s} of these cases are 1.0, 1.0, 1.0, 0.3 m, 0.3 days and 0.3 m, respectively. μ_{K_s} is 0.2592 m/d and the rainfall duration is 1 day.

The resultant reliability index β_i profiles for the four cases at $t = 0.2$ day, $t = 1$ day and $t = 2$ days, are displayed in Fig. 6a–c, respectively. The time periods, $t = 0.2$ day and $t = 2$ days, represent the

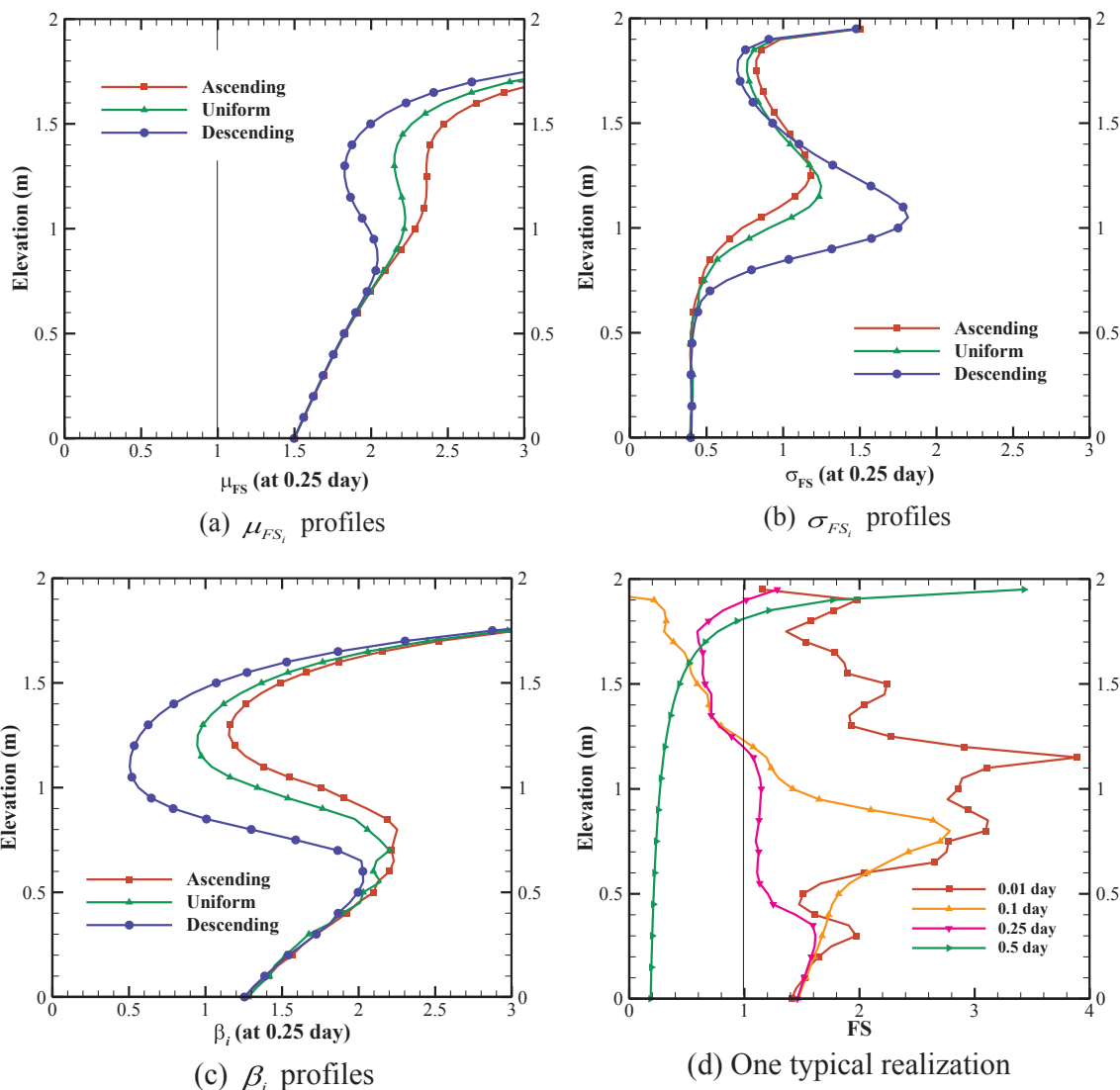


Fig. 7. μ_{FS_i} 's, σ_{FS_i} 's and β_i 's at different potential slip surfaces at the selected time ($t = 0.25$ day) under different rainfall patterns.

Table 2

Situations in which the uncertainties are likely to impact the reliability of slope stability evaluations.

Number	Conditions	Critical time	Low-reliability zone
1	Close to saturation	Early times	Any elevation of the slope
2	Unsaturated slope under heavy rainfalls	Early times	Shallow parts of the slope
3	Rainfall persists	Late times	near the impermeable bedrock
4	Rainfall has a descending trend	Early times	Shallow parts of the slope

time when the rain stops for SDIR and LDMR, respectively.

At 0.2 day, the rain stops in the case of SDIR while the rain continues in the case of LDMR. The resultant reliability profiles are plotted in Fig. 6a. The solid green lines with delta triangles and solid black lines with circles are for the LDMR cases with initial mean pressure heads of -2m and -3m , respectively. The reliabilities of the slope under LDMR are large. In spite of the initial mean pressure heads, SDIR leads to localized low-reliability zone at shallow depths of the slope as illustrated by the solid red lines with rectangles and solid blue lines with gradient triangles in the figure. Formation of this zone is expected since an intense rainfall leads to a decrease of the mean values of FS_i 's and large variations in slope stability (σ_{FS_i}) within short times (see Fig. 5).

At $t = 1$ day in Fig. 6b and $t = 2$ days in Fig. 6c, the reliabilities still maintain relatively high at shallow depths under LDMR, and the

reliabilities at shallow parts of the slope under SDIR rises due to the cease of rainfall and it becomes larger than those under LDMR. In addition, both SDIR and LDMR lead to a localized low-reliability zone at deep parts of the slope due to greater saturation. As a result, attention should be given to the uncertainties accumulated above the impermeable bedrock, where become critical to the slope stability evaluation, even if it is long after the heavy rainfall stops or under a mild rainfall. We show one typical realization of this situation in Fig. 6d, which is generated with abovementioned statistics under LDMR.

4.4. Effects of rainfall pattern

As reported by previous studies (e.g., Ng et al., 2001; Zhang et al., 2014), the rainfall pattern can significantly influence the slope stability

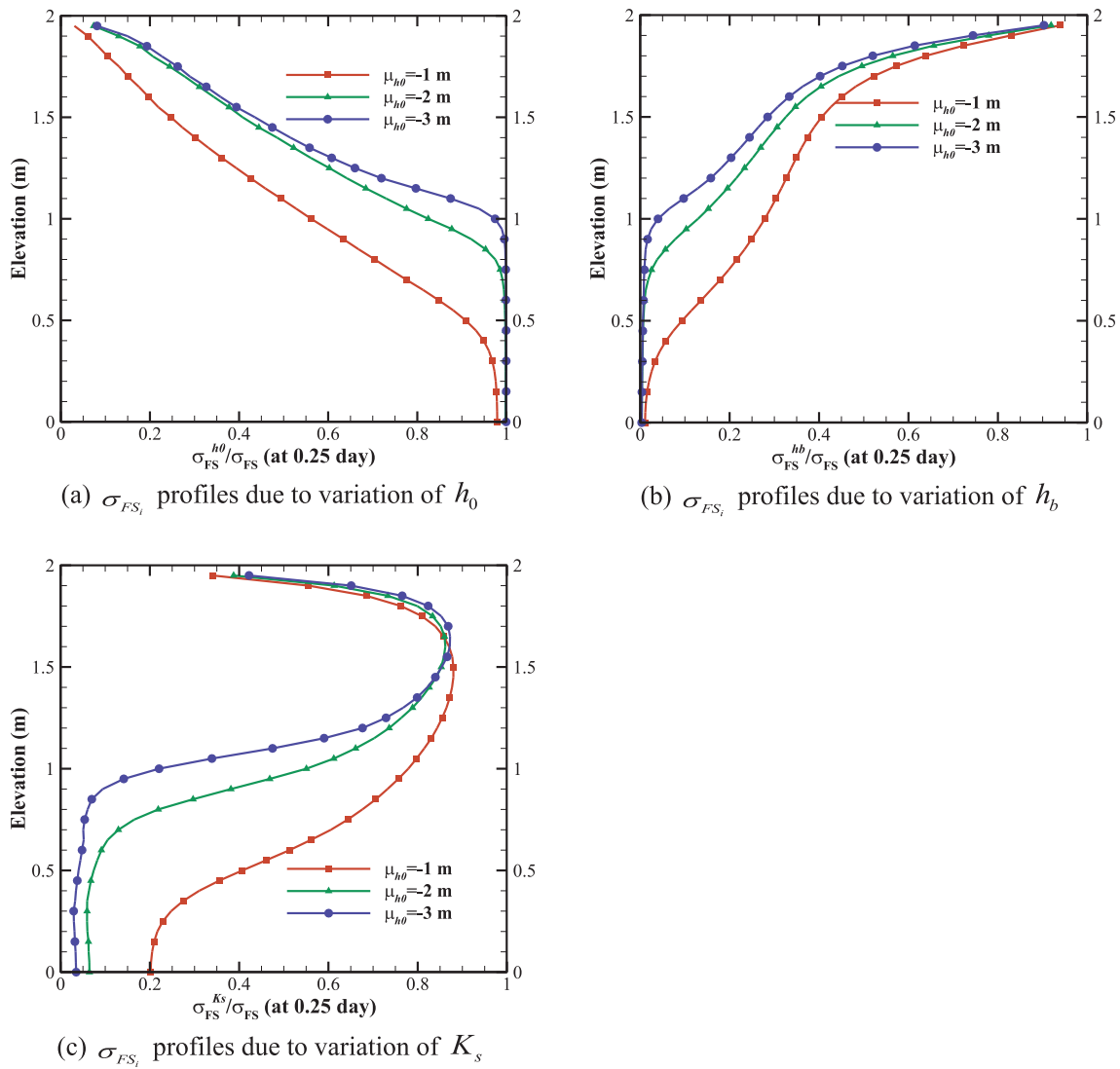


Fig. A1. Normalized σ_{FS_i} 's due to each parameter (h_0 , h_b and K_s) at different potential slip surfaces at the selected time ($t = 0.25$ day) with different mean initial pore water pressure distribution.

even when the rainfall amount is the same. For this reason, we examine the effects of rainfall pattern on slope reliability. Specifically, the stability, uncertainty, and reliability along the slope profile are calculated for three rainfall patterns (namely, ascending rainfall with μ_{hb} increasing from -0.2 to 0 m; uniform rainfall with μ_{hb} equals -0.1 m and descending rainfall with μ_{hb} decreasing from 0 to -0.2 m). The COV_{hb} 's of these three cases are set to the same, 1.0 . Note that in the case of ascending rainfall and the case of descending rainfall, μ_{hb} varies with times. Hence the COV_{hb} 's of these two cases are defined as the ratio of σ_{hb} to the value of μ_{hb} in the mid-time of the rainfall duration (i.e., 1 day). In addition, COV_{h_0} , COV_{K_s} , λ_{h_0} , λ_{hb} and λ_{K_s} of these cases are 1.0 , 1.0 , 0.3 m, 0.3 days and 0.3 m, respectively. μ_{h_0} is -2 m and μ_{K_s} is 0.2592 m/d.

The μ_{FS_i} profiles at $t = 0.25$ day under the three rainfall patterns are plotted in Fig. 7a. They indicate that the μ_{FS_i} profile corresponding to the descending rainfall is the closest to 1 at the upper part of the slope. The σ_{FS_i} profiles at $t = 0.25$ day under the three rainfall patterns are presented in Fig. 7b. The relative contribution from each parameter to σ_{FS_i} is shown in Fig. A3. As indicated by these figures, the rainfall pattern can significantly affect the distribution of the slope stability uncertainty. Both the propagation depth of σ_{FS_i} 's and the maximum value of the localized large-uncertainty zone corresponding to the descending rainfall are the largest among the three rainfall patterns at a

given time. The reliability index β_i profiles in Fig. 7c demonstrate that the descending rainfall pattern destabilizes slopes the most with the minimum value of the localized low-reliability zone. One typical realization generated with abovementioned statistics under the descending rainfall pattern is illustrated in Fig. 7d. These results are likely owing to the fact that the descending rainfall with large rainfall intensities at early time enhances infiltration and leads great uncertainties.

5. Conclusions

This study demonstrates that the uncertainties due to variabilities in initial soil pore water pressure distributions and rainfalls are as significant as that due to the variabilities in soil hydraulic properties, which have been emphasized by many previous studies. As a consequence, our study stresses the fact that to better evaluate the slope stability, the temporal and spatial propagation of slope stability uncertainty due to variabilities in initial soil pore water pressure distributions and rainfalls should also be considered.

In addition, this study demonstrates that the propagation of slope stability uncertainty is driven by the propagation of the mean flow field during the rainfall infiltration process. A localized large-uncertainty zone along the slope stability profile could form and lead to the existence of a localized low-reliability zone. Further, it demonstrates that

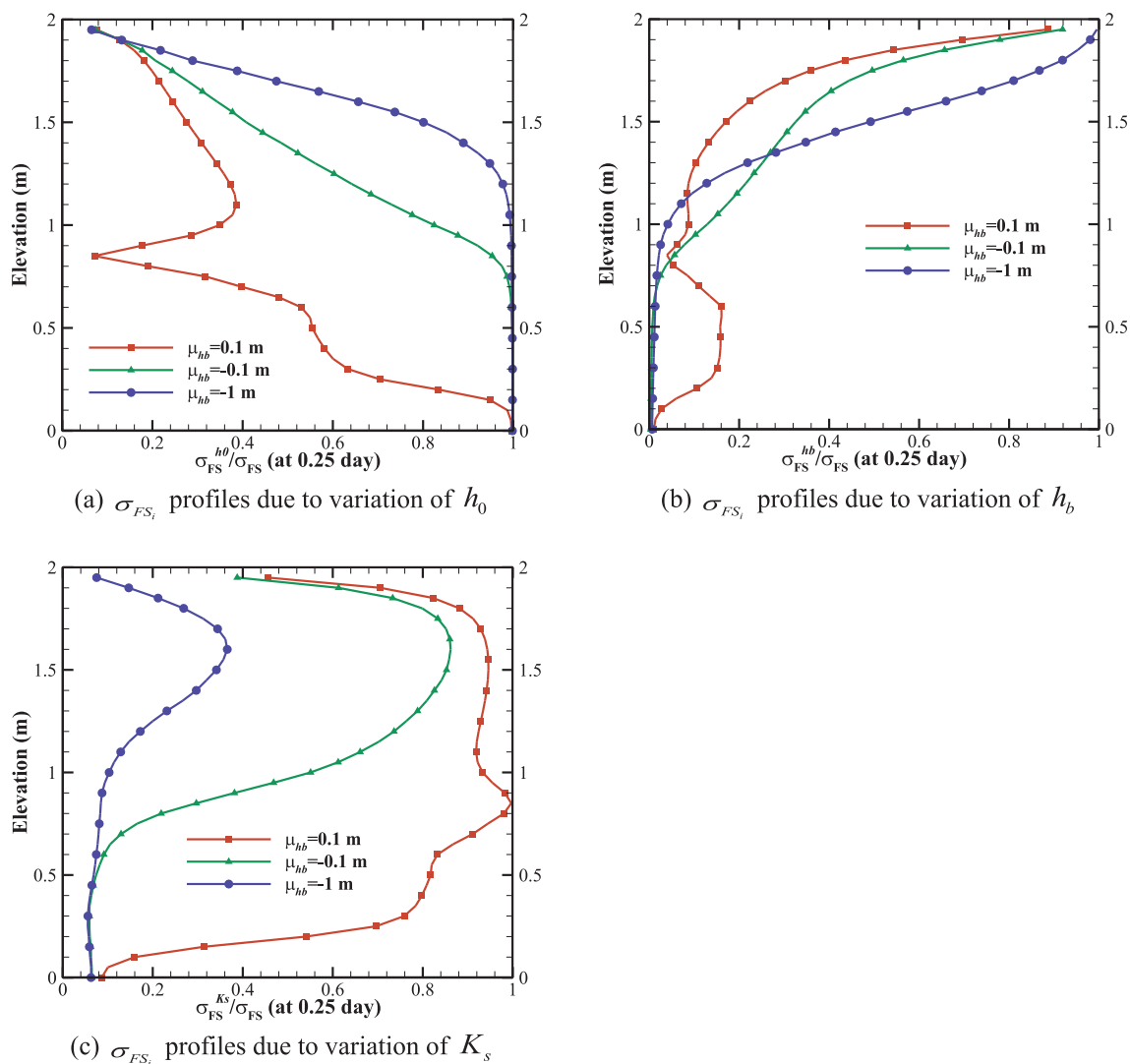


Fig. A2. Normalized σ_{FS_i} 's due to each parameter (h_0 , h_b and K_s) at different potential slip surfaces at the selected time ($t = 0.25$ day) under different rainfall intensities.

the build-up of the localized large-uncertainty zone or the localized low-reliability zone is greatly influenced by the prior knowledge of the mean of initial pore water pressure, the rainfall intensity, the rainfall duration, and the rainfall pattern.

The situations in which the uncertainties of slope stability are likely to impact the reliability of slope stability evaluations, along with the critical time and location are presented in Table 2. This indicates the location where the low-reliability zone forms and the time when this zone starts to impact the slope under different situations. Under such situations, the uncertainty plays a critical role in slope stability evaluation and requires special attention. That is, further investigation or monitoring measures should be implemented to the location of the low-reliability zone to reduce the uncertainty (e.g., Cai et al., 2017c). As a result, any unfavorable condition can be detected immediately before it is too late for prevention.

Note that the above analysis is based on one-dimensional infinite slope model such that the flow is restricted to vertical flow. For this reason, infiltrated water cannot detour from low K_s zones, and the pressure behind the zones must build up significantly to push water flow through. In other words, this one-dimensional flow may have amplified effects of hydraulic heterogeneity. Multi-dimensional flow models may reduce this magnification.

At last, the climate of a region dictates typical ranges of the soil moistures and rainfall intensity and rainfall duration during a specific season. Compiling historical records of spatial distribution of soil moistures and temporal variation of rainfalls at the region can yield the general statistical description of initial hydraulic conditions and rainfalls. This information could facilitate better evaluation of slope stability during any possible rainfall events.

Declaration of interest

None.

Acknowledgments

This work was supported by the National Natural Science Foundation of China (Grant No. 41807264); the Fundamental Research Funds for the Central Universities, China University of Geosciences (Wuhan) (Grant No. CUG170686); the China Scholarship Council (Grant No. 201406410032); the National Natural Science Foundation of China (Grant No. 41672313). The second author also acknowledges the Global Expert award through Tianjin Normal University from the Thousand Talents Plan of Tianjin City.

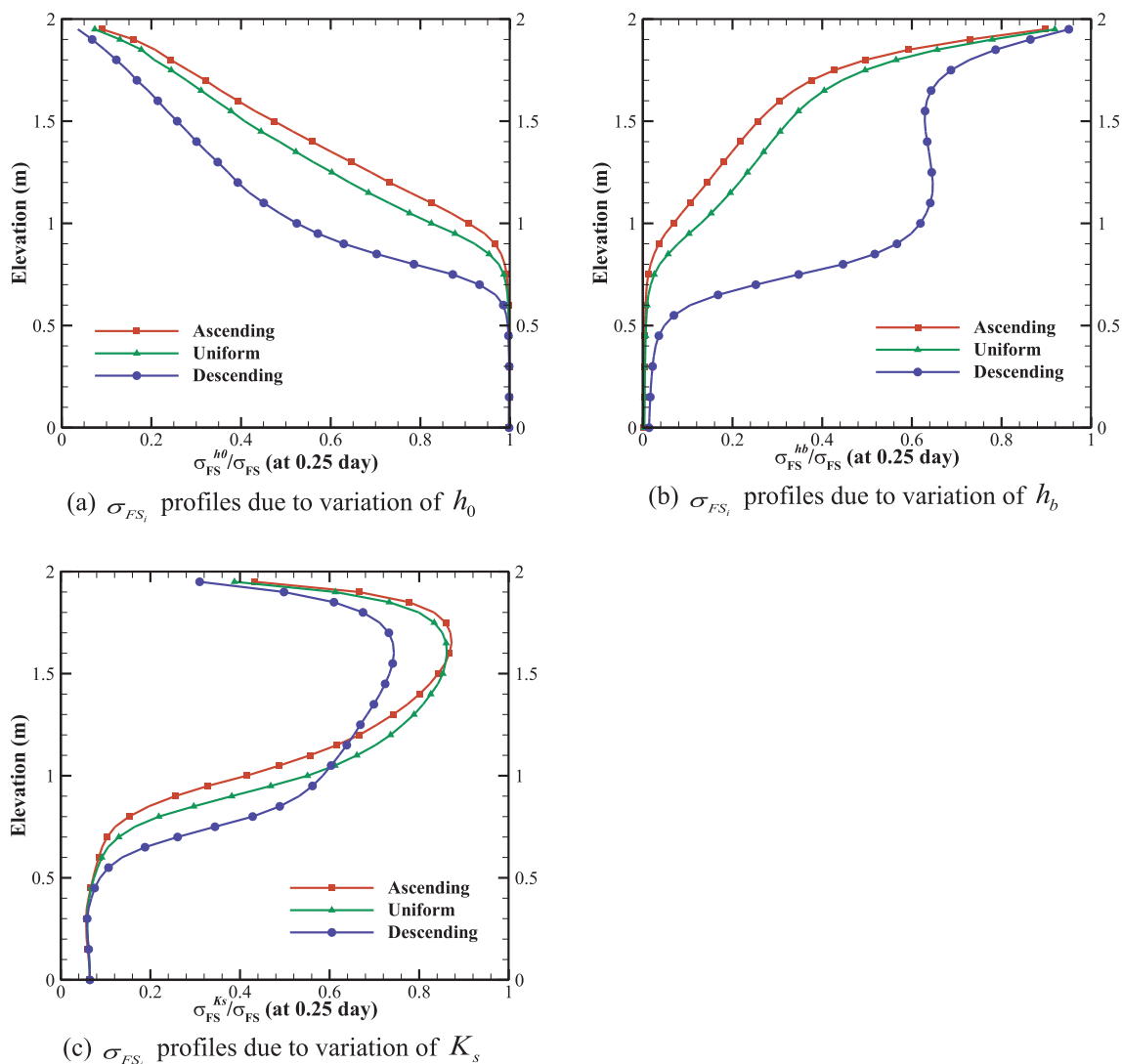


Fig. A3. Normalized σ_{FS_i} 's due to each parameter (h_0 , h_b and K_s) at different potential slip surfaces at the selected times under different rainfall patterns.

Appendix A

References

Ali, A., Huang, J., Lyamin, A.V., Sloan, S.W., Griffiths, D.V., Cassidy, M.J., Li, J.H., 2014. Simplified quantitative risk assessment of rainfall-induced landslides modelled by infinite slopes. *Eng. Geol.* 179, 102–116. <https://doi.org/10.1016/j.enggeo.2014.06.024>.

Brejda, J.J., Moorman, T.B., Smith, J.L., Karlen, D.L., Allan, D.L., Dao, T.H., 2000. Distribution and variability of surface soil properties at a regional scale. *Soil Sci. Soc. Am. J.* 64, 974. <https://doi.org/10.2136/sssaj2000.643974x>.

Cai, J.-S., Yan, E.-C., Yeh, T.-C.J., Zha, Y.-Y., Liang, Y., Huang, S.-Y., Wang, W.-K., Wen, J.-C., 2017a. Effect of spatial variability of shear strength on reliability of infinite slopes using analytical approach. *Comput. Geotech.* 81, 77–86. <https://doi.org/10.1016/j.compgeo.2016.07.012>.

Cai, J.-S., Yan, E.-C., Yeh, T.J., Zha, Y.-Y., 2017b. Sampling schemes for hillslope hydrologic processes and stability analysis based on cross-correlation analysis. *Hydrol. Process.* 31, 1301–1313. <https://doi.org/10.1002/hyp.11101>.

Cai, J.-S., Yan, E., Yeh, T.J., Zha, Y., 2016. Effects of heterogeneity distribution on hill-slope stability during rainfalls. *Water Sci. Eng.* 9, 134–144. <https://doi.org/10.1016/j.wse.2016.06.004>.

Cai, J.-S., Yeh, T.-C.J., Yan, E.-C., Tang, R.-X., Wen, J.-C., Huang, S.-Y., 2017c. An adaptive sampling approach to reduce uncertainty in slope stability analysis. *Landslides*. <https://doi.org/10.1007/s10346-017-0936-2>.

Cai, J.-S., Yeh, T.J., Yan, E.-C., Hao, Y.-H., Huang, S., Wen, J.-C., 2017d. Uncertainty of rainfall-induced landslides considering spatial variability of parameters. *Comput. Geotech.* 87, 149–162. <https://doi.org/10.1016/j.compgeo.2017.02.009>.

Cho, S.E., 2014. Probabilistic stability analysis of rainfall-induced landslides considering spatial variability of permeability. *Eng. Geol.* 171, 11–20. <https://doi.org/10.1016/j.enggeo.2013.12.015>.

Chowdhury, R., Flentje, P., 2002. Uncertainties in rainfall-induced landslide hazard. *Q. J. Eng. Geol. Hydrogeol.* 35, 61–69. <https://doi.org/10.1144/qjegh.35.1.61>.

Christian, J., Ladd, C., Baecher, G., 1994. Reliability and probability in stability analysis. *J. Geotech. Eng.* 120, 2180–2207.

D’Odorico, P., 2005. Potential for landsliding: dependence on hyetograph characteristics. *J. Geophys. Res.* 110, F01007. <https://doi.org/10.1029/2004JF000127>.

Fenton, G.A., Griffiths, D.V., 2008. *Risk Assessment in Geotechnical Engineering*. Wiley, New York.

Ghanem, R.G., Spanos, P.D., 1991. *Stochastic Finite Elements: A Spectral Approach*. Springer, New York.

Griffiths, D.V., Huang, J., Fenton, G.A., 2011. Probabilistic infinite slope analysis. *Comput. Geotech.* 38, 577–584. <https://doi.org/10.1016/j.compgeo.2011.03.006>.

Gui, S., Zhang, R., Turner, J.P., Xue, X., 2000. Probabilistic slope stability analysis with stochastic soil hydraulic conductivity. *J. Geotech. Geoenvironmental Eng.* 126, 1–9. [https://doi.org/10.1061/\(ASCE\)1090-0241\(2000\)126:1\(1\)](https://doi.org/10.1061/(ASCE)1090-0241(2000)126:1(1)).

Gupta, V.K., Waymire, E.C., 1993. A statistical analysis of mesoscale rainfall as a random cascade. *J. Appl. Meteorol.* 32, 251–267. [https://doi.org/10.1175/1520-0450\(1993\)032<0251:ASAOMR>2.0.CO;2](https://doi.org/10.1175/1520-0450(1993)032<0251:ASAOMR>2.0.CO;2).

Jiang, S.-H., Li, D.-Q., Cao, Z.-J., Zhou, C.-B., Phoon, K.-K., 2015. Efficient system reliability analysis of slope stability in spatially variable soils using monte carlo simulation. *J. Geotech. Geoenvironmental Eng.* 141, 04014096. <https://doi.org/10.1061/>

- (ASCE)GT.1943-5606.0001227.
- Li, D.-Q., Qi, X.-H., Phoon, K.-K., Zhang, L.-M., Zhou, C.-B., 2014. Effect of spatially variable shear strength parameters with linearly increasing mean trend on reliability of infinite slopes. *Struct. Saf.* 49, 45–55. <https://doi.org/10.1016/j.strusafe.2013.08.005>.
- Lu, N., Godt, J., 2008. Infinite slope stability under steady unsaturated seepage conditions. *Water Resour. Res.* 44, n/a-n/a. <https://doi.org/10.1029/2008WR006976>.
- Lu, Z., Zhang, D., 2007. Stochastic simulations for flow in nonstationary randomly heterogeneous porous media using a KL-based moment-equation approach. *Multiscale Model Simul.* <https://doi.org/10.1137/060665282>.
- Menabde, M., Sivapalan, M., 2000. Modeling of rainfall time series and extremes using bounded random cascades and levy-stable distributions. *Water Resour. Res.* 36, 3293–3300. <https://doi.org/10.1029/2000WR900197>.
- Minder, J.R., Roe, G.H., Montgomery, D.R., 2009. Spatial patterns of rainfall and shallow landslide susceptibility. *Water Resour. Res.* 45, 1–11. <https://doi.org/10.1029/2008WR007027>.
- Mualem, Y., 1976. A new model for predicting the hydraulic conductivity of unsaturated porous media. *Water Resour. Res.* 12, 513–522. <https://doi.org/10.1029/WR012i003p00513>.
- Ng, C.W., Shi, Q., 1998. A numerical investigation of the stability of unsaturated soil slopes subjected to transient seepage. *Comput. Geotech.* 22, 1–28. [https://doi.org/10.1016/S0266-352X\(97\)00036-0](https://doi.org/10.1016/S0266-352X(97)00036-0).
- Ng, C.W.W., Wang, B., Tung, Y.K., 2001. Three-dimensional numerical investigations of groundwater responses in an unsaturated slope subjected to various rainfall patterns. *Can. Geotech. J.* 38, 1049–1062. <https://doi.org/10.1139/cgj-38-5-1049>.
- Paolini, L., Villalba, R., Ricardo Grau, H., 2005. Precipitation variability and landslide occurrence in a subtropical mountain ecosystem of NW Argentina. *Dendrochronologia* 22, 175–180. <https://doi.org/10.1016/j.dendro.2005.06.001>.
- Parkin, T.B., Meisinger, J.J., Starr, J.L., Chester, S.T., Robinson, J.A., 1988. Evaluation of statistical estimation methods for lognormally distributed variables. *Soil Sci. Soc. Am. J.* 52, 323. <https://doi.org/10.2136/sssaj1988.03615995005200020004x>.
- Parkin, T.B., Robinson, J.A., 1992. Analysis of lognormal data. In: *Advances in Soil Science*. Springer, New York, pp. 193–235. https://doi.org/10.1007/978-1-4612-2930-8_4.
- Phoon, K.-K., Kulhawy, F.H., 1999. Characterization of geotechnical variability. *Can. Geotech. J.* 36, 612–624. <https://doi.org/10.1139/t99-038>.
- Stern, R.D., Coe, R., 1984. A model fitting analysis of daily rainfall data. *J. R. Stat. Soc. Ser. A* 147, 1. <https://doi.org/10.2307/2981736>.
- van Genuchten, M.T., 1980. A closed-form equation for predicting the hydraulic conductivity of unsaturated soils. *Soil Sci. Soc. Am. J.* 44, 892. <https://doi.org/10.2136/sssaj1980.03615995004400050002x>.
- von Ruethe, J., Lehmann, P., Or, D., 2014. Effects of rainfall spatial variability and intermittency on shallow landslide triggering patterns at a catchment scale. *Water Resour. Res.* 50, 7780–7799. <https://doi.org/10.1002/2013WR015122>.
- Yeh, T.-C., Khaleel, R., Carroll, K.C., 2015. *Flow Through Heterogeneous Geologic Media*. Cambridge University Press, New York.
- Yeh, T.J., Gelhar, L.W., Gutjahr, A.L., 1985a. Stochastic analysis of unsaturated flow in heterogeneous soils: 1 Statistically isotropic Media. *Water Resour. Res.* 21, 447–456. <https://doi.org/10.1029/WR021i004p00447>.
- Yeh, T.J., Gelhar, L.W., Gutjahr, A.L., 1985b. Stochastic analysis of unsaturated flow in heterogeneous Soils: 2. Statistically anisotropic media with variable α . *Water Resour. Res.* 21, 457–464. <https://doi.org/10.1029/WR021i004p00457>.
- Yeh, T.J., Gelhar, L.W., Gutjahr, A.L., 1985c. Stochastic analysis of unsaturated flow in heterogeneous soils: 3 Observations and applications. *Water Resour. Res.* 21, 465–471. <https://doi.org/10.1029/WR021i004p00465>.
- Yeh, T.J., Srivastava, R., Guzman, A., Harter, T., 1993. A numerical model for water flow and chemical transport in variably saturated porous media. *Ground Water* 31, 634–644. <https://doi.org/10.1111/j.1745-6584.1993.tb00597.x>.
- Zhang, J., Huang, H.W., Zhang, L.M., Zhu, H.H., Shi, B., 2014. Probabilistic prediction of rainfall-induced slope failure using a mechanics-based model. *Eng. Geol.* 168, 129–140. <https://doi.org/10.1016/j.enggeo.2013.11.005>.